

# Spectral function of a Luttinger liquid coupled to phonons and angle-resolved photoemission measurements in the cuprate superconductors

Ian P. Bindloss and Steven A. Kivelson

*Department of Physics, University of California, Los Angeles, California 90095-1547, USA*

(Dated: November 2, 2018)

We compute the finite-temperature single-particle spectral function of a one-dimensional Luttinger liquid coupled to an optical phonon band. The calculation is performed exactly for the case in which electron-phonon coupling is purely forward scattering. We extend the results to include backward scattering with a renormalization group treatment. The dispersion contains a change in velocity at the phonon energy, qualitatively similar to the case of electron-phonon coupling in a Fermi liquid. If the backward scattering part of the the electron-phonon interaction is not too strong compared to the forward scattering part, coupling to phonons also produces a pronounced peak in the spectral function at low energies. The calculated spectral function is remarkably similar to the angle-resolved photoemission spectra of the high-temperature superconductors, including the apparent presence of “nodal quasiparticles,” the presence of a “kink” in the dispersion, and the non-Fermi-liquid frequency and temperature dependencies. Although a microscopic justification has not been established for treating the electronic dynamics of the cuprates as quasi-one-dimensional, at the very least we take the quality of the comparison as evidence of the non-Fermi-liquid character of the measured spectra.

## I. INTRODUCTION

There is increasing, although controversial, experimental evidence that, in cuprate high-temperature superconductors, a strong coupling between electrons and optical phonons produces observable features in the single-hole spectral function  $A(\mathbf{k}, E)$  measured by angle-resolved photoemission spectroscopy (ARPES).<sup>1,2,3</sup> In attempting to understand the implications of these measurements, the experiments have been previously analyzed in the context of the theory of the electron-phonon (el-ph) coupling in a Fermi liquid. However, the observed spectral function exhibits a manifestly non-Fermi-liquid frequency and temperature dependence,<sup>4,5,6,7</sup> so the justification for this mode of analysis is not clear.

In the present paper, we compute and analyze the finite-temperature spectral function of a spinful, one-dimensional (1D) Luttinger liquid (LL) coupled to a dispersionless optical phonon band (Einstein phonon). Such a spectral function was computed previously in Ref. 8, but only at  $T = 0$  and in the absence of both electron-electron (el-el) interactions and el-ph backscattering. The LL is a quantum critical point, so the spectral function is a scaling function, and should be computed at finite temperature; the zero-temperature spectral function reveals only the high-frequency behavior of the scaling function. It is also essential to include el-el interactions, as in real materials they are typically much stronger than the el-ph interactions. Moreover, strong el-el interactions make qualitative changes to the “appearance” of the spectral function. The effects of phonon-assisted backward scattering are also important to consider, as we have done below.

Our motivation for this study is threefold. (1) There are a host of interesting quasi-1D materials,<sup>9,10</sup> some of which are amenable to ARPES studies,<sup>11,12,13</sup> to which this analysis may be directly applicable. (2) The LL is the theoretically best understood example of a non Fermi

liquid—just as many aspects of the Fermi liquid state are robust, independent of details of material and even dimensionality, we may hope that some features of non-Fermi-liquids are similarly generic, at least within classes of non-Fermi-liquids. In this case, the LL may serve as a paradigmatic model for a broader class of systems. (3) It may be the case that the quasi-2D cuprates have significant, self-organized “stripe” structures<sup>14</sup> which render them locally quasi-1D, in which case it may be possible to directly compare the results obtained here with experiments<sup>5</sup> in the cuprates and other highly correlated materials.<sup>15</sup>

Let us start with a qualitative summary of the solution of the el-ph problem in a Fermi liquid<sup>16</sup> at zero temperature. Consider the case of an optical phonon with frequency  $\omega_0$  and dimensionless el-ph coupling  $\lambda'$ , which is not too large. For  $|E| > \omega_0$ , the effect of the el-ph coupling on  $A(\mathbf{k}, E)$  is an  $E$ -independent broadening of the quasiparticle peak. For  $|E| \ll \omega_0$ , the phonons can be integrated out to produce new effective interactions in the Fermi liquid: the largest effect is a renormalization of the Fermi velocity,  $v_F \rightarrow v_F^* = v_F/(1 + \lambda') < v_F$ , while the most dramatic effect is the weak effective attraction produced between low-energy quasiparticles, which can lead to a superconducting instability of the Fermi liquid state.

We have computed the single-hole spectral function for a LL coupled to optical phonons for the case when the el-ph coupling does not produce a spin gap. We find that the same *words* describe the effects of the el-ph coupling as in the Fermi liquid case, but the results *look* quite different because the unperturbed LL spectral function is not a simple Lorentzian. Specifically, if we let  $\{g\}$  represent the set of coupling constants which define the LL (i.e. the charge and spin velocities  $v_c$  and  $v_s$ , and the corresponding Luttinger exponents  $K_c$  and  $K_s$ ), then our result can be summarized by

$$A(k, E) \sim \begin{cases} A_{LL}(k, E; \{g\}) + \dots & \text{for } |E| \gg \omega_0, \\ A_{LL}(k, E; \{g^*\}) & \text{for } |E| \ll \omega_0, \end{cases} \quad (1)$$

and there is a smooth crossover between the two limits when  $|E| \sim \omega_0$ . Here,  $A_{LL}$  is the spectral function of the pure LL (i.e. in the absence of el-ph coupling), the ellipsis represents perturbative corrections to the spectral function which can be ignored as long as the el-ph coupling is not too big or if  $|E|$  is high enough, and  $\{g^*\}$  are renormalized coupling constants obtained by integrating out the phonons—we give explicit expressions for these renormalized couplings below.

The principal results of the present paper are Eqs. (1) and (9). The latter is an analytic expression for the space-time spectral function that interpolates between the two limits in Eq. (1), and is shown to be very nearly exact in the exactly solvable case of forward scattering only. We later generalize it for el-ph couplings that include backscattering interactions. Plots of  $A(k, E)$  computed from Eq. (9) are shown in the figures.

There are several general features of  $A(k, E)$  that are worth noting. (1) As has been previously emphasized,<sup>5</sup> the spectral weight of the LL is concentrated in a roughly triangular region of the  $E$ - $k$  plane (see Fig. 7), reflecting the fractionalized character of the elementary excitations, in contrast to the Fermi liquid case in which the spectral weight is concentrated along the line  $E = v_F(k - k_F)$ , reflecting the quasiparticle dispersion. (2) There is a renormalization of the charge (holon) velocity produced by the el-ph coupling, such that  $v_c^* < v_c$ , which is analogous to the renormalization of  $v_F$  in the Fermi liquid. This produces a “kink” in the spectrum, as shown in Fig. 8. (3) The  $E$  dependence of  $A(\mathbf{k}, E)$  at fixed  $\mathbf{k}$  is referred to in the ARPES literature as the energy distribution curve (EDC), while the  $\mathbf{k}$  dependence at fixed  $E$  is referred to as the momentum distribution curve (MDC); the extent to which there is a quasiparticle-like peak in the EDC of a LL is strongly dependent on the value of  $K_c$ . For weakly interacting electrons,  $K_c \approx 1$ , and the EDC exhibits a peak, although this peak contains a power-law tail indicating the absence of fermionic quasiparticles. For strong repulsive interactions that are sufficiently long range,  $K_c \ll 1$ , in which case the EDC is extremely broad, and can even fail to exhibit any well defined peak near the Fermi energy. In contrast, the structure of the MDC is much less variable,<sup>5</sup> and remains peaked even for small  $K_c$ . The presence of extremely broad EDCs at the same time that the MDCs are narrow is a manifestly non-Fermi-liquid feature and a dramatic signature of the LL. This feature is illustrated in Fig. 13.

For a model with purely forward scattering el-ph interactions, and for more general couplings as long as the el-ph backscattering is not too strong, at low energies  $K_c$  is increased by the presence of el-ph interactions, i.e.  $K_c^* > K_c$ . For the physically relevant case when the bare  $K_c < 1$ , this means that features that are situated within  $\omega_0$  of the Fermi energy are made sharper (more peaked)

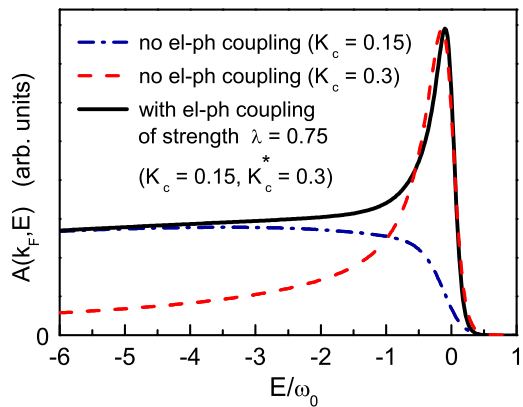


FIG. 1: Comparison of the single-hole spectral functions at  $k = k_F$  for a LL coupled to optical phonons (solid line), and a LL in absence of phonon coupling (dashed and dash-dotted lines). For the solid line, the el-ph coupling strength is  $\lambda = 0.75$  ( $v_c/v_c^* = K_c^*/K_c = 2$ ). For all curves,  $v_c/v_s = 4$  and  $\omega_0/T = 10$ . See the plot for the values of  $K_c$ . Normalizations are chosen for graphical clarity.

by the coupling to phonons. Therefore, for  $K_c \ll 1$ , the result has the following similarity with the Fermi liquid case: features in  $A(k, E)$  appear broader for binding energies above  $\omega_0$  than for binding energies below. In the Fermi liquid case, this comes from a phonon-induced broadening at high energies, but in the LL it comes from a phonon-induced narrowing at low energies.<sup>17</sup>

A plot of the EDC at  $k = k_F$  is shown in Fig. 1. The solid line shows  $A(k_F, E)$  for the case  $K_c = 0.15$ , in the presence of forward scattering el-ph coupling, which produces, at low energies, a renormalized  $K_c^* = 0.3$ . The dashed line shows  $A(k_F, E)$  for the pure LL, but with  $K_c = 0.3$ , while the dash-dotted line shows it for the pure LL with  $K_c = 0.15$ . Clearly, for the LL coupled to phonons, the renormalized  $K_c$  governs the properties at low binding energies, while the bare  $K_c$  dictates the behavior at large binding energies.

In Sec. II, we investigate the exactly solvable model (forward scattering only). The results are extended to general couplings using a renormalization group (RG) treatment in Sec. III. In Secs. IV and V we speculate on the relevance of these results to real materials, especially the high-temperature superconductors. Appendix A contains a derivation of the spectral function of the forward scattering only model. There we also present the exact result for the frequency- and momentum-dependent conductivity of this model. The optical conductivity is unchanged by the el-ph forward scattering, even though this interaction has dramatic effects on the spectral function. Appendix B contains technical details for the results presented in Sec. III.

## II. AN EXACTLY SOLVABLE MODEL

The model is defined by the Hamiltonian density

$$\mathcal{H} = \mathcal{H}_{\text{LL}} + \mathcal{H}_{\text{ph}} + \mathcal{H}_{\text{el-ph}}. \quad (2)$$

Here the purely electronic part of the Hamiltonian

$$\mathcal{H}_{\text{LL}} = \sum_{\alpha=c,s} \frac{v_\alpha}{2} \left[ K_\alpha \Pi_\alpha^2 + \frac{(\partial_x \phi_\alpha)^2}{K_\alpha} \right] \quad (3)$$

is the famous spin-charge-separated Tomonaga-Luttinger liquid model of the interacting one-dimensional electron gas (1DEG) at incommensurate filling. It is expressed via bosonization, in terms of bosonic charge ( $\alpha = c$ ) and spin ( $\alpha = s$ ) fields  $\phi_\alpha$ , and their canonically conjugate momenta  $\Pi_\alpha$ . Repulsive interactions usually renormalize the Luttinger parameter  $K_c$  below its noninteracting value of 1 such that  $0 < K_c < 1$ , and renormalize the velocities such that the  $v_s < v_F < v_c$ . We will assume the system is spin-rotation invariant, which dictates that  $K_s = 1$ . Expressions for the  $v_\alpha$ 's and  $K_\alpha$ 's in terms of microscopic short-range interaction parameters and reviews on the technique of bosonization can be found in many places in the literature.<sup>18,19,20,21,22</sup> Bosonization allows the fermionic fields to be expressed directly in terms of the bosonic fields:

$$\Psi_{\eta,\sigma} = \frac{e^{i\eta k_F x}}{\sqrt{2\pi a}} \exp \left\{ i\sqrt{\frac{\pi}{2}} [\eta(\phi_c + \sigma\phi_s) + \theta_c + \sigma\theta_s] \right\}, \quad (4)$$

where  $\Psi_{\eta,\sigma}$  is the right- or left-moving fermionic destruction field ( $\eta = \pm 1$ , respectively) for spin up or down ( $\sigma = \pm 1$ , respectively). Here  $\theta_\alpha(x) = -\int_{-\infty}^x dx' \Pi_\alpha(x')$  labels the dual bosonic field, and  $a$  is a short-distance cutoff corresponding to the lattice parameter. As is well known, the Hamiltonian in Eq. (3) describes a line of fixed points for interacting electrons, and so captures the essential low-energy physics of a large class of physical systems.

The purely vibrational part of the Hamiltonian

$$\mathcal{H}_{\text{ph}} = [P^2 + \omega_0^2 u^2] / 2M \quad (5)$$

describes an Einstein oscillator. Here  $u$  and  $P$  are the phonon field and its canonical conjugate momentum,  $M$  is the ion mass, and again  $\omega_0$  is the optical phonon frequency. Note that we work with units such that Boltzmann's and Planck's constants are  $k_B = \hbar = 1$ .

In the following section, we will consider a general form of the el-ph coupling,  $\mathcal{H}_{\text{el-ph}}$ , but for the purposes of the present section, we consider forward scattering interactions only,

$$\mathcal{H}_{\text{el-ph}} = \alpha_2 u \hat{\rho} = \alpha_2 \sqrt{2/\pi} u (\partial_x \phi_c), \quad (6)$$

where  $\alpha_2$  is the el-ph coupling parameter,  $\hat{\rho}$  is the long-wavelength component of the charge density, and the second equality makes use of the standard bosonization expression for  $\hat{\rho}$ . The forward scattering model is exactly solvable since in its bosonized form it is quadratic

in the fields. In Appendix A we compute the renormalized couplings that define the  $\{g^*\}$  for this model. The exact result is

$$v_c^* = v_c \sqrt{1 - \lambda}, \quad K_c^* = \frac{K_c}{\sqrt{1 - \lambda}}, \quad (7)$$

where

$$\lambda = \frac{2K_c \alpha_2^2}{\pi v_c M \omega_0^2}, \quad (8)$$

and the spin couplings are unrenormalized. Note that  $\lambda$  depends on both the el-ph and el-el interactions. Also note that  $v_c/v_c^* = K_c^*/K_c \geq 1$ . At low energies,  $v_c$  is reduced due to ‘‘phonon drag,’’ while  $K_c$  is increased due to an attractive interaction mediated by phonons. Since this model possesses an instability at  $\lambda = 1$ , where the charge velocity goes to zero,  $\lambda$  is restricted to the range  $0 \leq \lambda < 1$ . The analog of this instability for the case of coupling to *acoustic* phonons has been studied previously.<sup>23</sup>

In Appendix A we derive an exact expression for the spectral function. This quantity is most easily expressed in position space, but even then involves a momentum integral in the exponent that cannot be performed analytically. The integral can be evaluated numerically, and fortunately we are able to derive a simple analytic expression that accurately approximates it, as shown in Appendix A and Fig. 15. We therefore use this analytic approximation in subsequent calculations.

Specifically, our analytic approximation for the single-hole Green's function  $G_\eta(x, t; \lambda) = \langle \Psi_{\eta,\sigma}^\dagger(x, t) \Psi_{\eta,\sigma}(0, 0) \rangle$  is

$$G_\eta(x, t; \lambda) \approx G_\eta(x, t; 0) \frac{g_\eta(x, t; v_c^*, K_c^*, v_c/\omega_0)}{g_\eta(x, t; v_c, K_c, v_c/\omega_0)}, \quad (9)$$

where the exact Green's function in the absence of phonon coupling  $G_\eta(x, t; 0)$  at temperature  $T = 1/\beta$  is<sup>24</sup>

$$G_\eta(x, t; 0) = \frac{e^{-i\eta k_F x}}{2\pi a} \prod_{\alpha=c,s} g_\eta(x, t; v_\alpha, K_\alpha, a), \quad (10)$$

and we have defined the function

$$g_\eta(x, t; v, K, a) = \prod_{j=\pm 1} \left\{ \frac{iv\beta}{\pi a} \sinh \left[ \frac{\pi(vt + j\eta x - ia)}{v\beta} \right] \right\}^{-(K-j)^2/8K} \quad (11)$$

Equation (9) is the central result of this paper. The spectral function measured by ARPES is accurately given by its Fourier transform.

Specifically, the single-hole spectral function for right-moving fermions is<sup>25</sup>

$$A(k, E) = \int_{-\infty}^{\infty} dx \int_{-\infty}^{\infty} dt e^{i(kx - Et)} G_1(x, t; \lambda). \quad (12)$$

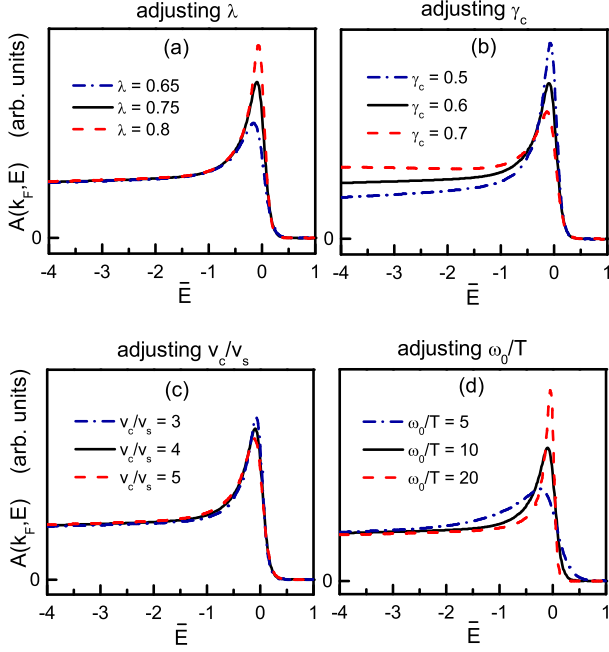


FIG. 2: Dependence of the EDC at  $k = k_F$  on  $\lambda$ ,  $\gamma_c$ ,  $v_c/v_s$ , and  $\omega_0/T$  [(a), (b), (c), and (d) respectively]. In each panel, only one parameter is varied, and the rest are held fixed. Unless otherwise labeled,  $\lambda = 0.75$ ,  $\gamma_c = 0.6$ ,  $v_c/v_s = 4$ , and  $\omega_0/T = 10$ . For example, for the curves in (a),  $\lambda$  has the value labeled in the plot legend, while  $\gamma_c = 0.6$ ,  $v_c/v_s = 4$ , and  $\omega_0/T = 10$ . In (a), the values of  $v_c/v_c^* = K_c^*/K_c$  are 1.69, 2, 2.24 for  $\lambda$  equal to 0.65, 0.75, 0.8, respectively. In (b),  $K_c$  is 0.172, 0.150, 0.134 for  $\gamma_c$  equal to 0.5, 0.6, 0.7, respectively. Normalizations are chosen for graphical clarity (the apparent variation of the total spectral weight is an artifact).

By combining this with Eq. (9), one obtains

$$A(k, E) \approx \frac{\bar{\beta}^2}{\pi \bar{a} \omega_0} \int_{-\infty}^{\infty} d\tilde{x} \int_0^{\infty} d\tilde{t} \chi(\tilde{x}, \tilde{t}) \times \cos[\bar{\beta}(\bar{k}\tilde{x} - \bar{E}\tilde{t}) - \Theta(\tilde{x}, \tilde{t})], \quad (13)$$

where we defined the dimensionless quantities  $\bar{\beta} = \omega_0 \beta / \pi$ ,  $\bar{a} = a \omega_0 / v_c$ ,

$$\bar{k} = v_c(k - k_F) / \omega_0, \quad \bar{E} = E / \omega_0, \quad (14)$$

and the functions

$$\chi(\tilde{x}, \tilde{t}) = \prod_{i=1}^4 \prod_{j=\pm 1} \left[ \frac{(a_i/v_i)^2}{\sinh^2(\tilde{t} + j\tilde{x}/v_i) + \sin^2(a_i/v_i)} \right]^{\gamma_{ij}/2} \quad (15)$$

and

$$\Theta(\tilde{x}, \tilde{t}) = \sum_{i=1}^4 \sum_{j=\pm 1} \gamma_{ij} \arctan \left[ \frac{\tanh(\tilde{t} + j\tilde{x}/v_i)}{\tan(a_i/v_i)} \right], \quad (16)$$

with

$$\gamma_{ij} = (1 - 2\delta_{i3}) \frac{(K_i - j)^2}{8K_i}, \quad (17)$$

$$K_1 = 1, \quad K_2 = K_3 = K_c, \quad K_4 = K_c^*, \quad (18)$$

$$v_1 = v_s/v_c, \quad v_2 = v_3 = 1, \quad v_4 = v_c^*/v_c, \quad (19)$$

$$a_1 = a_2 = \bar{a}/\bar{\beta}, \quad a_3 = a_4 = 1/\bar{\beta}. \quad (20)$$

Above,  $\tilde{x}$  and  $\tilde{t}$  are dimensionless dummy variables of integration,  $\delta_{i3}$  is the Kronecker delta, and  $\bar{a} \ll 1$  is a dimensionless cutoff. The spectral function plots were obtained by performing the double integration in Eq. (13) numerically. Henceforth, we adopt the notation

$$\gamma_c \equiv (K_c + K_c^{-1} - 2)/8 = \gamma_{21}, \quad (21)$$

which vanishes in the absence of el-el interactions.

$A(k, E)$  depends only on  $\bar{k}$ ,  $\bar{E}$ ,  $\omega_0/T$ , and on the three dimensionless parameters  $\lambda$ ,  $\gamma_c$ , and  $v_c/v_s$ .<sup>26</sup> In order to provide the reader with a qualitative understanding of how the spectral function depends on these parameters, in Fig. 2 we show how the EDC at  $k = k_F$  changes when one is varied with the rest held fixed. Henceforth, we either chose representative parameters for the figures, or, for cases in which the theory is compared to experimental data, we fit the parameters. Not surprisingly, for cases in which we have fitted the parameters, they turn out to be somewhat material dependent.

Figure 3(a) exhibits the temperature dependence of the EDC at  $k = k_F$ . The spectral weight of the low energy peak is reduced by increasing  $T$ , while at the same time the width of the peak increases proportional to  $T$ , due to the quantum critical nature of the LL. The value  $\gamma_c = 0.6$  ( $K_c \approx 0.15$ ) used here indicates strong el-el repulsion.

In Fig. 4 we show the dependence of the EDCs on  $\bar{k}$ , with and without forward scattering coupling to phonons, for  $\omega_0/T = 10$  and  $\gamma_c = 0.6$ . Note the ‘‘double-peak’’ structure present near the phonon energy for moderate values of  $\bar{k}$ .

Figure 5 shows MDCs at various values of  $\bar{E}$  for the same parameters as Fig. 4. A similar plot is shown in Fig. 6 at a lower temperature ( $\omega_0/T = 40$ ). Because of the lower temperature, here one can resolve *three* local maxima for moderate values of  $\bar{E}$ . As shown in Fig. 6(c), which is an enlargement of the  $\bar{E} = -1$  curve, the center local maximum disperses at the renormalized charge velocity  $v_c^*$ . Since this peak is by far the dominant one for  $|\bar{E}| \ll 1$ , the low-energy dispersion is characterized by what appears to be a single peak dispersing with velocity  $v_c^*$ . At higher  $|\bar{E}|$ , the  $v_c^*$  peak disappears. If the temperature is increased sufficiently, the three local maxima can no longer be resolved and appear as one peak, as seen in Fig. 5(a). Also note that phonon coupling creates larger spectral weight at the spinon velocity  $v_s$ , due to the higher effective  $K_c$  (this feature disappears at high binding energies).

In Fig. 7 we present contour plots in the  $\bar{E}$ - $\bar{k}$  plane, with and without phonon coupling, for the same parameters as Fig. 4. Note the pronounced peak (red spot) at low binding energies in Fig. 7(a), due to the increase in the effective  $K_c$ . The reduction in charge velocity at low binding energies can also be seen here.

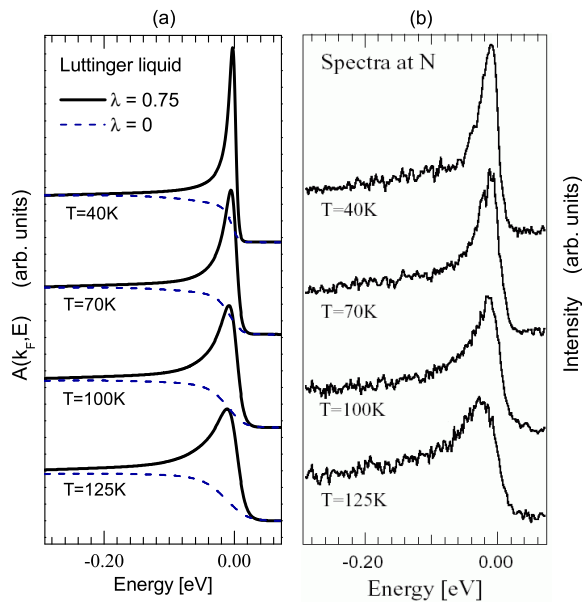


FIG. 3: Comparison of the temperature dependence of the EDCs at  $k = k_F$  for (a) a LL coupled to phonons and (b) ARPES data of optimally doped Bi2212 ( $T_c = 89$  K) at the Fermi surface crossing along  $\mathbf{k} = (0, 0)$  to  $(\pi, \pi)$  (the nodal direction) (Ref. 34). In (a),  $\omega_0 = 70$  meV,  $\gamma_c = 0.6$ , and  $v_c/v_s = 4$ . The solid line is for  $\lambda = 0.75$ , and the dashed line is the result for the pure LL.

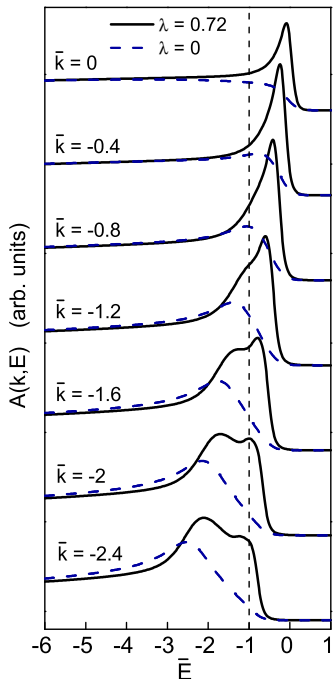


FIG. 4: EDCs with (solid lines) and without (dashed lines) forward scattering coupling to phonons of strength  $\lambda = 0.72$  ( $v_c/v_c^* = K_c^*/K_c = 1.9$ ), with  $\gamma_c = 0.6$ ,  $v_c/v_s = 3$ , and  $\omega_0/T = 10$ . The notation  $\bar{k} = v_c(k - k_F)/\omega_0$  and  $\bar{E} = E/\omega_0$ , where  $E$  is measured with respect to the Fermi energy. The curves have vertical offsets proportional to  $\bar{k}$ .

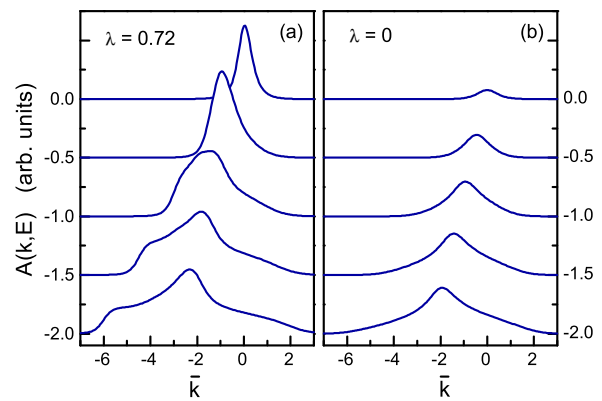


FIG. 5: MDCs (a) with and (b) without coupling to phonons of strength  $\lambda = 0.72$  for  $\omega_0/T = 10$ . All parameters are the same as Fig. 4. The curves are offset by  $\bar{E}$ .

Figure 8 shows the dispersion in the  $\bar{E}$ - $\bar{k}$  plane, determined by fitting MDC curves to Lorentzian functions (the same method used in the ARPES literature). A change in the slope occurs at  $\bar{E} \approx -1$ . The ratio of the slope at  $|\bar{E}| \ll 1$  to the slope at  $|\bar{E}| \gg 1$  is approximately  $v_c^*/v_c = \sqrt{1 - \lambda}$ . Note that the dispersion, when determined by fitting to Lorentzians, is weakly  $T$  dependent.

### III. GENERAL ELECTRON-PHONON COUPLING

In general, both forward and backward scattering (i.e. with momentum transfer near  $2k_F$ ) are possible. Thus, in general, we should consider both processes:

$$\mathcal{H}_{\text{el-ph}} = u \left[ \alpha_2 \hat{\rho} + \alpha_1 \sum_{\sigma} \left( \Psi_{1,\sigma}^{\dagger} \Psi_{-1,\sigma} + \text{H.c.} \right) \right]. \quad (22)$$

In this case, because  $\Psi$  is a nonlinear function of the bosonic fields, the problem is not exactly solvable. We therefore treat the backscattering term  $\alpha_1$  with a perturbative renormalization group scheme. It is important to note that if  $\alpha_1$  is sufficiently strong, a gap opens up in the spin sector, and the system is a Luther-Emery liquid<sup>27</sup> (LEL) instead of a LL (see Appendix B). We refer the reader to Ref. 28 for a detailed study of the phase boundary separating the LL and LEL phases. Here we limit ourselves to the case in which the spectrum is gapless.

It is convenient to define the dimensionless el-ph couplings

$$\lambda_1 = \frac{\alpha_1^2}{\pi v_F M \omega_0^2}, \quad \lambda_2 = \frac{\alpha_2^2}{\pi v_F M \omega_0^2}. \quad (23)$$

In Appendix B we derive the following relations, which are generalizations of Eq. (7) to the case of nonzero  $\lambda_1$ :

$$v_c^* = v_c \sqrt{(1 - \Lambda)(1 - \lambda + K_c^2 \Lambda)}, \quad (24)$$

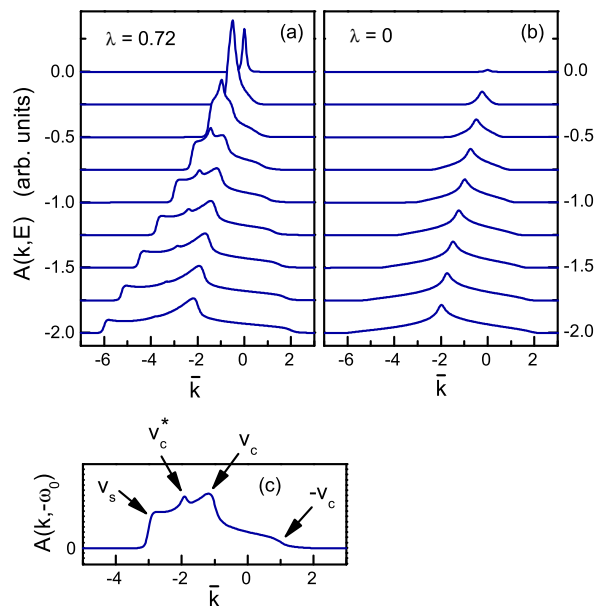


FIG. 6: MDCs (a) with and (b) without coupling to phonons for  $\omega_0/T = 40$  and the same interaction strengths as Fig. 4. (c) shows an enlargement of the  $\bar{E} = -1$  curve from (a), and labels the velocities at which various features disperse. In (a) and (b) the curves are offset by  $\bar{E}$ .

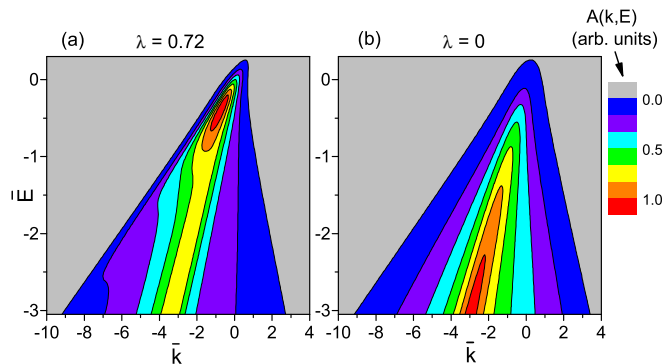


FIG. 7: Contour plot for  $\omega_0/T = 10$  of the single-hole spectral function (a) with and (b) without forward scattering to phonons of strength  $\lambda = 0.72$ . All parameters are the same as in Fig. 4.

$$K_c^* = K_c \sqrt{\frac{1 - \Lambda}{1 - \lambda + K_c^2 \Lambda}}, \quad (25)$$

where we have introduced the effective backscattering el-ph parameter

$$\Lambda = \frac{v_F}{2K_c v_c} \lambda_1^*, \quad (26)$$

which lies in the range  $0 \leq \Lambda < 1$ . Here  $\lambda_1^*$  is the renormalized value of the bare el-ph backscattering parameter  $\lambda_1$ . For the case in which the el-ph interaction is unretarded (when the Fermi energy  $E_F < \omega_0$ ),  $\lambda_1$  remains unrenormalized ( $\lambda_1^* = \lambda_1$ ). However, for the phys-

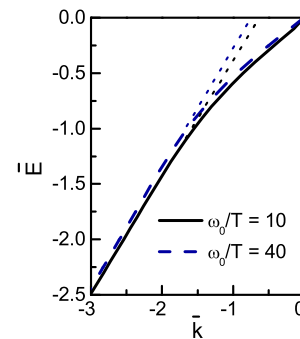


FIG. 8: Dispersion for  $\lambda = 0.72$ , determined by fitting MDCs to Lorentzians, for  $\omega_0/T = 10$  (solid line) and  $\omega_0/T = 40$  (dashed line). Interaction strengths are the same as in Fig. 4. The dotted lines are fits to the high- $|\bar{E}|$  portion of the dispersions.

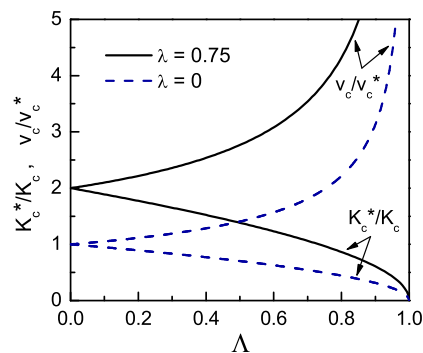


FIG. 9: Dependence of the magnitude of the kink ( $v_c/v_c^*$ ) and the degree to which the spectral function is peaked at low energies compared to high energies ( $K_c^*/K_c$ ) on the effective backscattering el-ph interaction parameter  $\Lambda$ , for the case  $K_c = 0.15$ . The dashed lines are the result in the absence of forward scattering el-ph interaction ( $\lambda = 0$ ), while the solid lines are for  $\lambda = 0.75$ .

ically interesting case  $E_F > \omega_0$ ,  $\lambda_1^*$  depends on the ratio  $E_F/\omega_0$  and on the strength of the el-el interactions (see Appendix B for an explicit relation). As before, the forward scattering el-ph parameter is  $\lambda = (2K_c v_F/v_c) \lambda_2$ ; note that  $\lambda_2$  contains no asterisk because it remains unrenormalized regardless of  $E_F/\omega_0$ .<sup>29</sup>

Equations (24) and (25) are actually completely general, nonperturbative expressions. However, our only way of relating the effective parameter  $\Lambda$  to the microscopic parameter  $\lambda_1$  is through Eq. (B6), which was obtained from one-loop RG, and is therefore valid only when the el-el interactions are weak and  $\lambda_1 \ll 1$ . But Eqs. (24) and (25) remain valid even if the RG is carried out to an infinite number of loops.

If fitting to particular ARPES data, the parameters  $K_c$ ,  $K_c^*$ , and  $v_c^*/v_c$  are easily obtained. Then,  $\lambda$  and  $\Lambda$  can be determined by inverting Eqs. (24) and (25). Therefore, for quasi-1D systems, ARPES is an effective probe of the relative amounts of forward and (renormal-

ized) backward scattering el-ph interactions.

Note that for nonzero  $\Lambda$ , the relation  $K_c^*/K_c = v_c/v_c^*$  no longer holds; instead  $K_c^*/K_c = (1 - \Lambda)v_c/v_c^*$ . For  $K_c < 1$ , the relation  $v_c^* < v_c$  holds regardless of  $\Lambda$  and  $\lambda$ . However,  $K_c^* > K_c$  holds only if the ratio  $\Lambda/\lambda$  is small enough. Specifically, if  $\Lambda/\lambda > 1/(1+K_c^2)$ , then  $K_c^* < K_c$ , which means that the low-energy spectral features are no longer made more peaked due to phonons. Figure 9 illustrates the result of increasing  $\Lambda$  at fixed  $\lambda$ , for the case  $K_c = 0.15$ . The magnitude of the kink, given by  $v_c/v_c^*$ , is *increased* by turning up  $\Lambda$ , while  $K_c^*$  is reduced. For all the spectral function plots in this paper, we have set  $\Lambda = 0$ .

#### IV. COMPARISONS WITH ARPES EXPERIMENTS IN THE CUPRATES

In this section, we wish to illustrate the extent to which the observed ARPES spectra in the cuprate superconductors resemble those of a LL coupled to optical phonons. At a gross level, the character of the resemblance between the observed spectrum and a pure LL was established in Ref. 5. The strength of this analogy is further supported<sup>13</sup> by direct comparison between the experimentally measured  $A(k, E)$  in a quasi-1D bronze and the cuprates. However, as more and better data have become available, it has become clear that there are features in the cuprate data—especially the widely reported “kinks” in the dispersion of the MDC peaks<sup>1,2,30,31,32</sup>—that are qualitatively absent from the pure LL. The pure LL is also unable to reproduce the “nodal quasiparticles” seen in experiments while simultaneously producing broad features at high energy. Here, therefore, we propose to make a comparison between the measured spectral functions, and the spectral function of a LL coupled to an optical phonon.<sup>33</sup> Since the LL describes a gapless state, we only compare our results to data taken in the gapless “nodal” direction, which is defined as  $\mathbf{k} = (0, 0)$  to  $(\pi, \pi)$ . In other directions, the ARPES spectrum of the cuprates develops a gap below a certain temperature, whereas the spectrum remains gapless in the nodal direction even in the superconducting state.

In Fig. 3 we have fitted the theoretical EDCs to ARPES data<sup>7</sup> in optimally doped  $\text{Bi}_2\text{Sr}_2\text{CaCu}_2\text{O}_{8+\delta}$  ( $\text{Bi2212}$ )<sup>34</sup> at the Fermi surface crossing in the nodal direction, shown at various temperatures, both above and below  $T_c$ . The experimental temperature dependence has been previously interpreted as evidence for quantum critical behavior. Since the LL is a quantum critical state, the resemblance between theory and experiment in the present paper supports this interpretation.

Figure 10 presents a fit to normal state EDCs for slightly underdoped<sup>1</sup>  $\text{Bi2212}$  along the nodal direction, at various momenta. The theoretical curves contain a similar double-peak structure as the experiment. The line shapes of both the theory and experiment are characterized by extremely long high energy tails.

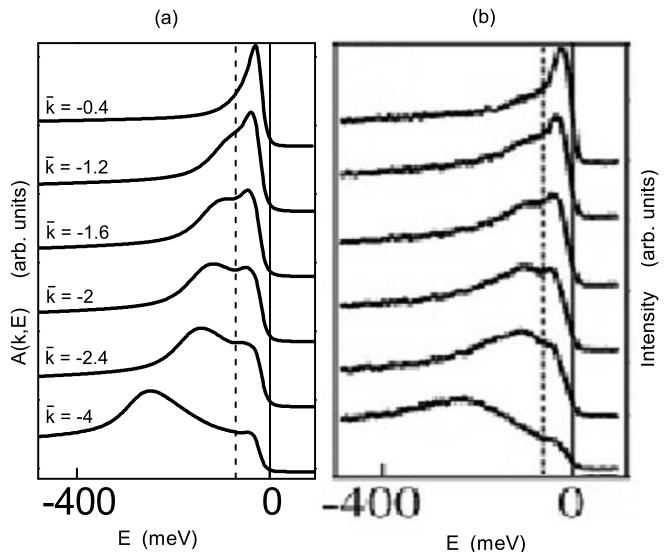


FIG. 10: Comparison of EDCs for (a) a LL coupled to phonons and (b) ARPES data of slightly underdoped  $\text{Bi2212}$  along the nodal direction ( $T_c = 84$  K) at various momenta (Ref. 1). For (a),  $\lambda = 0.72$ ,  $\gamma_c = 0.6$ ,  $v_c/v_s = 3$ ,  $\omega_0 = 70$  meV,  $T = 80$  K, and the dashed line is drawn at  $|E| = \omega_0$ .

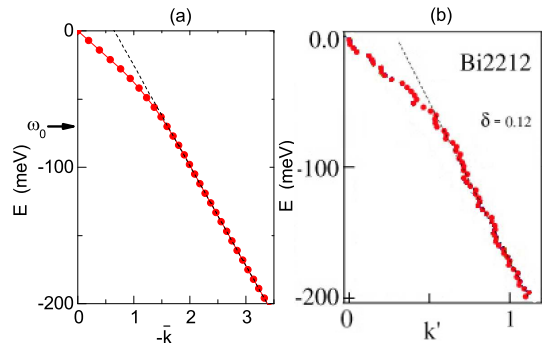


FIG. 11: Comparison of the dispersion of (a) the LL coupled to phonons with  $\omega_0 = 70$  meV at  $T = 30$  K to (b) the dispersion in  $\text{Bi2212}$  ( $T_c = 84$  K) at  $T = 30$  K in the nodal direction (Ref. 1). For (a), all interaction strengths are the same as in Fig. 10. For both plots, the dispersion was obtained by fitting MDC curves to Lorentzians. In (b), the authors define the rescaled momentum  $k'$ , by normalizing to 1 the value of  $k_F - k$  at  $E = -170$  meV. The dashed lines are guides to the eye.

Figure 11(a) shows the theoretical dispersion for the same parameters as Fig. 10(a), except with  $T = 30$  K, determined by fitting the theoretical MDCs to Lorentzians. Fig. 11(b) shows the experimental dispersion for slightly underdoped<sup>1</sup>  $\text{Bi2212}$  in the nodal direction at  $T = 30$  K, which the authors obtained with the same fitting procedure. The bizarre feature of the experimental data in which the dispersion at high binding energies does not extrapolate to the origin is also seen in the theory.<sup>35</sup>

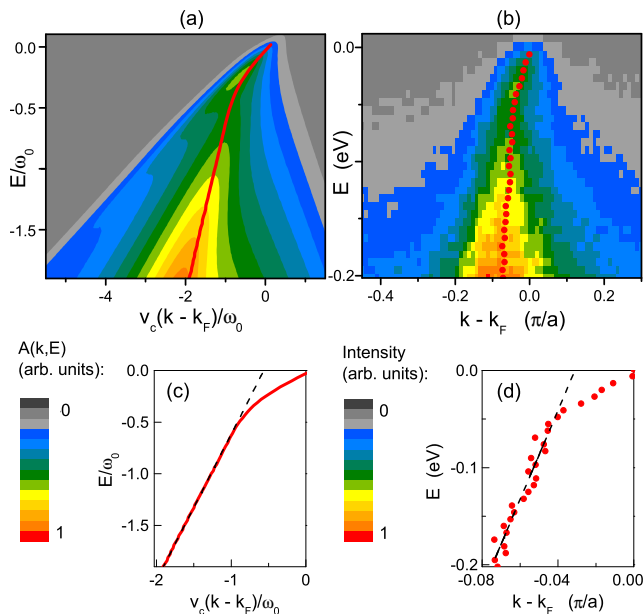


FIG. 12: Comparison of intensity plot of (a) the single-hole spectral function of a LL coupled to phonons with  $\gamma_c = 1.5$ ,  $\lambda = 0.93$ ,  $\omega_0/T = 20$ , and  $v_c/v_s = 3$  to (b) the ARPES spectrum of nonsuperconducting LSCO (3% doping) at  $T = 30$  K (Ref. 36). In (a) and (b), the red line and points are the dispersion, obtained by fitting MDCs to Lorentzians. Panels (c) and (d) show enlargements of the dispersions; the dashed lines are fits to the high-binding-energy portion.

For the theory plots, the manner by which the dispersion is extracted (least-squares fitting to Lorentzians), yields a weighted average of the *four* velocities labeled in Fig. 6(c). It is the contribution from the velocity  $-v_c$  that is responsible for the plotted high-energy dispersion not extrapolating to the origin at  $E = 0$  and  $k = k_F$ . This is because, when the dispersion is determined by fits to Lorentzians, the presence of spectral weight at  $k > k_F$  [near the right side of the triangle in Fig. 12(a)] “pulls” the high-binding-energy dispersion to higher velocities.

Figure 12(a) shows a contour plot of the theoretical spectral function in the  $\bar{E}$ - $\bar{k}$  plane and compares it to ARPES data<sup>36</sup> for underdoped, nonsuperconducting  $\text{La}_{2-x}\text{Sr}_x\text{CuO}_4$  (LSCO) with  $x = 0.03$  [Fig. 12(b)]. The value of  $\lambda$  was chosen to give  $v_c/v_c^* = K_c^*/K_c = 3.8$ , which is the same as the ratio of the high to low binding energy velocities in the experimental plot. In Figs. 12(c) and 12(d) we show the dispersions, obtained in the same manner as in Fig. 11. The EDCs and MDCs from these plots, at the Fermi momentum and Fermi energy, respectively, are shown explicitly in Fig. 13. For both the theory and experiment, the contrast between the sharpness of the MDCs and the breadth of the EDCs is dramatic.

Note that the large values of  $\gamma_c$  and large values of  $\lambda$  used for all the theoretical plots above indicate the presence of very strong el-el and el-ph interactions, with an effective el-ph interaction that is peaked in the forward scattering direction (since we used  $\Lambda = 0$ ).

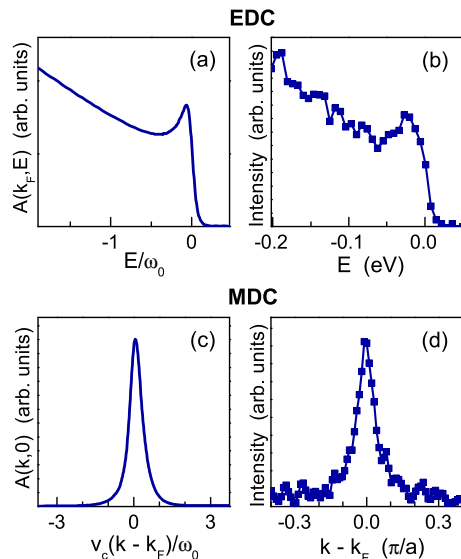


FIG. 13: EDC at  $k = k_F$  for (a) LL coupled to phonons and (b) underdoped nonsuperconducting LSCO (Ref. 36) (nodal direction); and MDC at  $E = 0$  for (c) LL coupled to phonons and (d) underdoped LSCO (nodal direction). Panels (a) and (c) are slices from the plot in Fig. 12(a); (b) and (d) are slices from the data in Fig. 12(b).

In Refs. 37 and 38, an effort is made to fit the experimental dispersion of the cuprates to the conventional theory of el-ph coupling in a Fermi liquid. Both papers report that getting a good fit to the experimental kink requires coupling between electrons and a broad spectrum of phonon modes that extends all the way up to two or three hundred meV. As the authors point out, this is unphysical, since from neutron scattering, the highest-energy phonon mode is less than 100 meV in all of the cuprates. This suggests that either phonons are not responsible for the kink, or if they are, that the correct theory is very different from the conventional Fermi liquid one. In the present paper, the phonon density of states that couples to electrons is a single  $\delta$  function at  $\omega_0$  (Einstein phonon). But even treating the phonon density of states as adjustable, we suspect that a Fermi liquid treatment would not be able to fit the frequency and temperature dependence of the spectral function, nor the linear dependence of the MDC width on energy.<sup>7</sup>

## V. CONCLUSIONS

We have analyzed the effect of the el-ph coupling on the single-particle spectral function of the theoretically best understood (and exactly solvable) non-Fermi-liquid, the LL. Since, by definition, a non-Fermi-liquid is a state in which the elementary excitations are not simply dressed electrons or holes,  $A(\mathbf{k}, E)$  should be the measurable quantity in which non-Fermi-liquid effects are most dramatic. Thus, it is important to have a clear idea of which

features of this function best distinguish a Fermi liquid from a non-Fermi-liquid. It has been argued previously<sup>5</sup> that the most dramatic signature of a LL is the appearance of extremely broad tails in the EDC, although peaks in the MDC remain relatively sharp. (This signature is particularly dramatic when the el-el interactions are strong; while the same distinction applies *in principle* for weak interactions, *in practice* the LL is harder to distinguish from a Fermi liquid when the couplings are weak.)

We have shown that some of the gross characteristic features of el-ph coupling in a Fermi liquid—an apparent kink in the dispersion relations and EDCs that are more peaked at  $|E| < \omega_0$  compared to  $|E| > \omega_0$ —are also present in a LL with strong el-el repulsion and forward scattering coupling to phonons. For a LL with more general el-ph couplings, the kink is still present, but the tendency of the EDC to be more peaked for  $|E| < \omega_0$  is eliminated by sufficiently strong el-ph backscattering. However, in either case, the Fermi liquid analogy cannot be taken too far: The basic discrepancy between the sharpness of the MDCs and the breadth of the EDCs, and the “triangular” confinement of spectral weight in the  $E$ - $k$  plane, remain striking aspects of the LL which differentiate it from the Fermi liquid.

We have also shown examples of measured spectral functions in the cuprates, and drawn attention to the similarities between them and our theoretical results. We believe that the similarities are dramatic. Exactly why the measured spectral functions look so much like the LL coupled to phonons is a deep question, which we will not explore further, here. However, at the very least, we feel that this comparison reinforces the conclusion, which has certainly been reached<sup>4,5,6,7</sup> on the basis of a variety of other experimental observations in the cuprates, that these materials are not well described in terms of the conventional electronic quasiparticles of simple metals.

### Acknowledgments

We wish to thank J. Allen, N. P. Armitage, P. Johnson, T. Valla, S. Sachdev, G. H. Gweon, E. Arrigoni, D. Orgad, Z.-X. Shen, V. Oganesyan, J. Tranquada, and A. Lanzara for useful discussions, and X. J. Zhou for supplying the data in Fig. 12(b). This work was supported, in part, by the National Science Foundation Grant No. DMR 01-10329 (S.A.K.) and by the Department of Energy Contract No. DE-FG03-00ER45798 (I.P.B.).

### APPENDIX A: THE SPECTRAL FUNCTION AND CONDUCTIVITY OF THE EXACTLY SOLVABLE MODEL

We now derive the spectral function of the model with purely forward scattering interactions. We work in the Matsubara representation, in which  $\tau = it$  is the imaginary time, and the partition functional is represented as

a path integral over the bosonic fields  $\Pi_c, \phi_c, \Pi_s, \phi_s, P$ , and  $u$ . Since the Lagrangian is quadratic in all of these fields, we can integrate out all fields except  $\phi_c$  and  $\phi_s$ . This results in the Lagrangian  $\mathcal{L} = \mathcal{L}_c[\varphi_c] + \mathcal{L}_s[\varphi_s]$  with

$$\mathcal{L}_c[\varphi_c] = \frac{1}{2K_c v_c} \left[ \omega_n^2 + v_c^2 q^2 - \lambda \frac{\omega_0^2 v_c^2 q^2}{\omega_n^2 + \omega_0^2} \right] |\varphi_c|^2, \quad (\text{A1})$$

$$\mathcal{L}_s[\varphi_s] = \frac{1}{2K_s v_s} [\omega_n^2 + v_s^2 q^2] |\varphi_s|^2. \quad (\text{A2})$$

Here the bosonic Matsubara frequency is  $\omega_n = 2\pi n/\beta$ , the field  $\varphi_\alpha = \varphi_\alpha(q, \omega_n)$  is defined by  $\phi_\alpha(x, \tau) = (2\pi\beta L)^{-1} \sum_n \int dq e^{-i\omega_n \tau + iqx} \varphi_\alpha(q, \omega_n)$ , and  $L$  is the length of the system. The partition functional is then given by the path integral  $Z = \int \mathcal{D}\varphi_c \mathcal{D}\varphi_s e^{-S_c[\varphi_c] - S_s[\varphi_s]}$  with  $S_\alpha[\varphi_\alpha] = (2\pi\beta L)^{-1} \sum_n \int dq \mathcal{L}_\alpha[\varphi_\alpha]$ . The zero-temperature dispersion relations for the hybridized charge-phonon bosonic collective modes are thus

$$\omega_\pm = \left[ \frac{\omega_0^2 + v_c^2 q^2 \pm \sqrt{(\omega_0^2 - v_c^2 q^2)^2 + 4\lambda\omega_0^2 v_c^2 q^2}}{2} \right]^{1/2}. \quad (\text{A3})$$

Note that for  $\lambda = 0$ ,  $\omega_- = v_c q$  is the long-wavelength density mode of the LL, and  $\omega_+ = \omega_0$  is the Einstein phonon mode. In Fig. 14(a), we plot  $\omega_-$  and  $\omega_+$  for various values of  $\lambda$ .

It is a general feature of the bosonization approach that the fermionic correlation functions are most simply expressed as a function of space and time. The Matsubara space-time Green’s function was previously computed for a LL with forward scattering interactions with acoustic (instead of optical) phonons.<sup>39,40</sup> The analytic structure of Eq. (A1) differs from the acoustic phonon model according to  $\omega_0 \rightarrow cq$ , where  $c$  is the velocity of the acoustic phonon. The initial steps for computing the space-time Green’s function involving functional integration over the fields and Matsubara frequency summations are the same for our model, except for this “parameter” change. We will therefore not reproduce these steps here, but rather refer the reader to Ref. 39. The final momentum integral done in the exponent, however, is different for the two models.

We write the single-particle imaginary-time Green’s function for right moving fermions  $\mathcal{G}(x, \tau; \lambda) = -\langle T_\tau \Psi_{1,\sigma}(x, \tau) \Psi_{1,\sigma}^\dagger(0, 0) \rangle$ , where  $T_\tau$  is the imaginary time ordering operator, as

$$\mathcal{G}(x, \tau; \lambda) = -\frac{e^{ik_F x}}{2\pi a} \exp[-f_c(\bar{x}, \bar{\tau}; \lambda) - f_s(\bar{x}, \bar{\tau})] \quad (\text{A4})$$

(results for left-moving fermions are obtained by changing  $x \rightarrow -x$ ). Here  $f_c$  and  $f_s$  are the charge and spin contributions to the exponent, which we will write in terms of the dimensionless variables  $\bar{x} = x\omega_0/v_c$  and  $\bar{\tau} = \omega_0 \tau$ . To simplify notation, for now we express the result in the limit  $T \rightarrow 0$ . For  $\tau > 0$  and infinitely large system

length, the exact result is

$$f_c(\bar{x}, \bar{\tau}; \lambda) = \int_0^\infty d\bar{q} e^{-\bar{a}\bar{q}} \sum_{\nu=\pm} \{ \mathcal{A}_\nu [1 - \cos(\bar{q}\bar{x}) e^{-\bar{\omega}_\nu \bar{\tau}}] - i \mathcal{B}_\nu \sin(\bar{q}\bar{x}) e^{-\bar{\omega}_\nu \bar{\tau}} \}, \quad (\text{A5})$$

$$f_s(\bar{x}, \bar{\tau}) = F(\bar{x}, \bar{\tau}; v_s/v_c, K_s, \bar{a}), \quad (\text{A6})$$

where  $\bar{a} = a\omega_0/v_c$  and we defined the functions

$$\mathcal{A}_\pm = \frac{(K_c^2 + 1)(\bar{\omega}_\pm^2 - 1) + \lambda}{4K_c\bar{\omega}_\pm(\bar{\omega}_\pm^2 - \bar{\omega}_\mp^2)}, \quad (\text{A7})$$

$$\mathcal{B}_\pm = \frac{\bar{\omega}_\pm^2 - 1}{2\bar{q}(\bar{\omega}_\pm^2 - \bar{\omega}_\mp^2)}, \quad (\text{A8})$$

$$\bar{\omega}_\pm^2 = \frac{1 + \bar{q}^2 \pm \sqrt{(1 - \bar{q}^2)^2 + 4\lambda\bar{q}^2}}{2}, \quad (\text{A9})$$

and

$$F(\bar{x}, \bar{\tau}; v, K, a) = \frac{1}{8} \left( K + \frac{1}{K} \right) \ln \left[ \frac{\bar{x}^2 + (a + v\bar{\tau})^2}{a^2} \right] - \frac{i}{2} \arctan \left[ \frac{\bar{x}}{a + v\bar{\tau}} \right]. \quad (\text{A10})$$

For  $\lambda = 0$ , the charge and spin parts are the same after an appropriate change of parameters:

$$f_c(\bar{x}, \bar{\tau}; 0) = F(\bar{x}, \bar{\tau}; 1, K_c, \bar{a}), \quad (\text{A11})$$

yielding the known<sup>24</sup> Green's function of a pure LL

$$\mathcal{G}(x, \tau; 0) = -\frac{e^{ik_F x}}{2\pi a} \prod_{\alpha=c,s} H(x, \tau; v_\alpha, K_\alpha, a), \quad (\text{A12})$$

where

$$H(x, \tau; v, K, a) = \left[ \frac{a^2}{(a + v\tau)^2 + x^2} \right]^{(K-1)^2/8K} \sqrt{\frac{a}{a + v\tau - ix}}. \quad (\text{A13})$$

For arbitrary values of the parameters, although it is straightforward to evaluate Eq. (A5) numerically, it does not appear possible to perform the integration analytically. We were, however, able to perform it analytically for the case of arbitrary  $\lambda$  but  $\bar{a} \gg 1$ :

$$\mathcal{G}(x, \tau; \lambda) = -\frac{e^{ik_F x}}{2\pi a} H(x, \tau; v_c^*, K_c^*, a) H(x, \tau; v_s, K_s, a) \quad \text{for } \bar{a} \gg 1, \quad (\text{A14})$$

with  $v_c^*$  and  $K_c^*$  given by Eq. (7). The limit  $\bar{a} \gg 1$  is typically not satisfied in real materials, but since the spectral function is independent of  $\bar{a}$  for  $|\bar{k}|, |\bar{E}| \ll 1/\bar{a}$ , we can use Eq. (A14) to deduce the exact behavior of the spectral function in the limit  $|\bar{k}|, |\bar{E}| \ll 1$ , regardless of the value of  $\bar{a}$ :

$$A(k, E; \lambda) \propto A_{LL}(k, E; v_c^*, K_c^*, v_s, K_s) \text{ for } |E| \ll \omega_0, \quad (\text{A15})$$

where  $A_{LL}(k, E; v_c, K_c, v_s, K_s) = A(k, E; 0)$  is the spectral function of the pure Luttinger liquid.

For the physically interesting case  $\bar{a} \ll 1$ , we were able to derive an accurate analytic approximation for Eq. (A5), which is the following:

$$f_c(\bar{x}, \bar{\tau}; \lambda) \approx f_c(\bar{x}, \bar{\tau}; 0) + F(\bar{x}, \bar{\tau}; v_c^*/v_c, K_c^*, 1) - F(\bar{x}, \bar{\tau}; 1, K_c, 1), \quad (\text{A16})$$

which gives for the Green's function

$$\mathcal{G}(x, \tau; \lambda) \approx \mathcal{G}(x, \tau; 0) \frac{H(x, \tau; v_c^*, K_c^*, v_c/\omega_0)}{H(x, \tau; v_c, K_c, v_c/\omega_0)} \quad \text{for } \bar{a} \ll 1, \quad (\text{A17})$$

with  $v_c^*$  and  $K_c^*$  given again by Eq. (7). The  $T \neq 0$  single-hole real-time Green's function is written, using this approximation, in Eq. (9).

We demonstrate the accuracy of this analytic approximation by comparing Eq. (A16) with the exact result, obtained by performing the integration in Eq. (A5) numerically. From Figs. 15(c) and 15(d) we see that for  $\lambda = 0.75$  and  $\gamma_c = 0.6$ , the approximation gives within 9% of the exact result for the real part of  $f_c(\bar{x}, \bar{\tau}; \lambda)$ . For  $\lambda = 0.25$  [Figs. 15(a) and 15(b)], the error is less than 3%. The agreement with the imaginary part is similarly excellent.

We have also computed the frequency- and momentum-dependent conductivity for the LL with forward scattering off phonons. The exact result for the real part of the conductivity at  $T = 0$  is

$$\sigma_1(q, \omega; \lambda) = e^2 K_c v_c \sum_{\nu=\pm 1} [W \delta(\omega - \nu\omega_+) + (1 - W) \delta(\omega - \nu\omega_-)]. \quad (\text{A18})$$

Here  $e$  is the charge of the electron,  $\delta$  is the delta function, and the spectral weight of the  $\omega_+$  mode is

$$W = \frac{\omega_+^2 - \omega_0^2}{\omega_+^2 - \omega_-^2}, \quad (\text{A19})$$

which depends only on  $v_c q/\omega_0$  and  $\lambda$ . We plot  $W$  in Fig. 14(b). Note that the conductivity at  $q = 0$  (optical conductivity) remains unchanged by forward scattering off phonons:

$$\sigma_1(0, \omega; \lambda) = \sigma_1(0, \omega; 0) = 2e^2 K_c v_c \delta(\omega), \quad (\text{A20})$$

yet this same interaction produces dramatic changes to the spectral function.

## APPENDIX B: RG TREATMENT OF GENERAL ELECTRON-PHONON COUPLING

In the case in which the el-el couplings and the backscattering el-ph coupling  $\lambda_1$  [Eq. (23)] are weak,

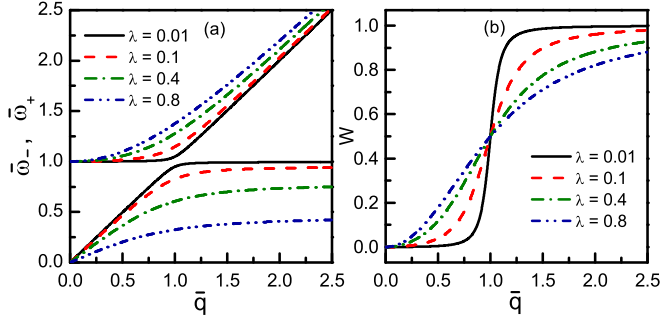


FIG. 14: Panel (a) shows the dispersion of the bosonic modes  $\omega_+$  (upper curves) and  $\omega_-$  (lower curves). (b) shows the spectral weight  $W$  of the  $\omega_+$  mode in the conductivity. The notation is  $\bar{\omega}_\pm = \omega_\pm/\omega_0$  and  $\bar{q} = v_c q/\omega_0$ .

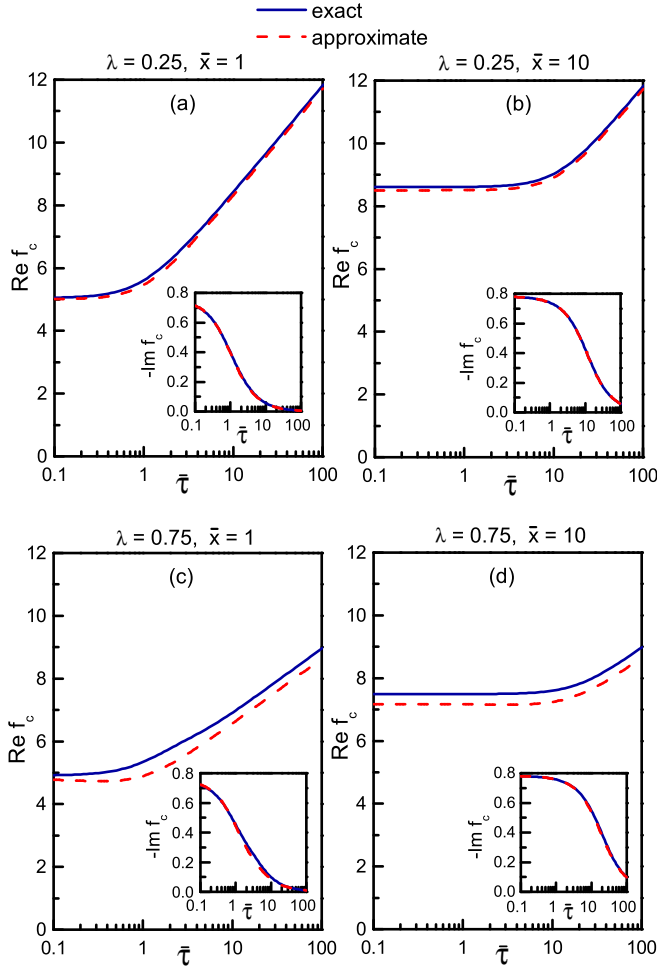


FIG. 15: Comparison of the exact Green's function charge exponent  $f_c(\bar{x}, \bar{\tau}; \lambda)$ , obtained by evaluating Eq. (A5) numerically (solid lines), with the approximate analytic expression in Eq. (A16) (dashed lines). Panels (a) and (b) are for  $\lambda = 0.25$ ; (c) and (d) are for  $\lambda = 0.75$ . For all panels,  $\gamma_c = 0.6$  and  $\bar{a} = 0.05$ . Panels (a) and (c) show the  $\bar{\tau}$  dependence for  $\bar{x} = 1$ ; (b) and (d) are for  $\bar{x} = 10$ . The main plots show the real part of  $f_c$  and the insets show the imaginary part. For the imaginary part, the dashed and solid lines overlap.

although of arbitrary relative strength, the phonon-induced renormalization of the LL parameters can be computed using a two-step perturbative (one-loop) RG scheme.<sup>28,41,42</sup> Since, for  $E_F \gg \omega_0$ , the coupling  $\lambda_1$  is strongly renormalized, and the RG flows of  $\lambda_1$  are modified by the direct el-el interactions, the resulting expressions for the renormalizations of  $v_c$  and  $K_c$  are more complicated than in Eq. (7). However, they have recently been analyzed in detail by one of us,<sup>28</sup> and will be summarized below.

We employ standard notation for the important short-range el-el interaction parameters of the incommensurate 1DEG:  $g_1$  (backscattering),  $g_2$  (forward scattering on both left- and right-moving branches), and  $g_4$  (forward scattering on only one branch). The Hamiltonian density for the el-el interaction portion is then

$$\begin{aligned} \mathcal{H}_{\text{el-el}} = & g_1 \sum_{\sigma, \sigma' = \pm 1} \Psi_{1, \sigma}^\dagger \Psi_{-1, \sigma'}^\dagger \Psi_{1, \sigma'} \Psi_{-1, \sigma} \\ & + g_2 \sum_{\sigma, \sigma' = \pm 1} \Psi_{1, \sigma}^\dagger \Psi_{-1, \sigma'}^\dagger \Psi_{-1, \sigma'} \Psi_{1, \sigma} \\ & + g_4 \sum_{\eta, \sigma = \pm 1} \Psi_{\eta, \sigma}^\dagger \Psi_{\eta, -\sigma}^\dagger \Psi_{\eta, -\sigma} \Psi_{\eta, \sigma}. \end{aligned} \quad (\text{B1})$$

For the extended Hubbard model in the continuum (weak-coupling) limit, these parameters are  $g_1 = U - 2V'$ ,  $g_2 = U + 2V'$ , and  $g_4 = U/2 + 2V'$ , where  $U$  is the onsite interaction,  $V' = -V \cos(2k_F)$ , and  $V$  is the nearest neighbor interaction (near half-filling,  $V' \approx V$ ).

For an incommensurate 1DEG in the presence of a general el-ph coupling, the effective charge parameters at low energy are

$$v_c^* = v_F \sqrt{(1 + g_4^{\text{tot}})^2 - (g_c^{\text{tot}}/2)^2}, \quad (\text{B2})$$

$$K_c^* = \sqrt{\frac{1 + g_4^{\text{tot}} + g_c^{\text{tot}}/2}{1 + g_4^{\text{tot}} - g_c^{\text{tot}}/2}}, \quad (\text{B3})$$

where we defined

$$g_c^{\text{tot}} = \bar{g}_1 - 2\bar{g}_2 - (\lambda_1^* - 2\lambda_2), \quad (\text{B4})$$

$$g_4^{\text{tot}} = \bar{g}_4 - \lambda_2, \quad (\text{B5})$$

and  $\bar{g}_i = g_i/\pi v_F$ . Here the renormalized el-ph backscattering coupling is denoted by  $\lambda_1^*$ . For the case  $E_F \gg \omega_0$  and  $\bar{g}_1, \bar{g}_2, \lambda_1 \ll 1$ , it is given by<sup>28</sup>

$$\lambda_1^* = \frac{\lambda_1 h(l_0)}{1 - \lambda_1 \int_0^{l_0} dx h(x)}, \quad (\text{B6})$$

where

$$h(x) = \frac{\exp[-(\bar{g}_1 - 2\bar{g}_2)x/2]}{(1 + \bar{g}_1 x)^{3/2}}, \quad (\text{B7})$$

$l_0 \equiv \ln(E_F/\omega_0)$ , and  $\lambda_1$  and  $\lambda_2$  are the bare el-ph couplings defined in Eq. (23).

In the weak-coupling limit and for  $E_F \gg \omega_0$ , the total effective backscattering interaction after integrating out degrees of freedom from  $E_F$  to  $\omega_0$  is given by

$$g_1^{\text{tot}} = \frac{\bar{g}_1}{1 + \bar{g}_1 l_0} - \lambda_1^*. \quad (\text{B8})$$

In order for the Luttinger liquid description to be valid, it is required that  $g_1^{\text{tot}}$  is repulsive ( $g_1^{\text{tot}} > 0$ ). In this case, the effective spin parameters are  $K_s^* = 1$  and  $v_s^* = v_F(1 - \bar{g}_4)$ . However, if  $\lambda_1^*$  is large enough to cause  $g_1^{\text{tot}} < 0$ , the RG flows carry  $K_s^*$  and  $v_s^*$  to zero at low energies, signaling the emergence of a spin gap. In this case, the system is described as a Luther-Emery liquid<sup>27</sup> phase.

We refer the reader to Ref. 28 for a detailed study of the phase diagram of the 1DEG coupled to phonons. Since the spectral function computed in the present paper is not applicable to a Luther-Emery liquid, here we restrict our attention to the case in which there is no spin gap.

By combining the above expressions for  $v_c^*$  and  $K_c^*$  with the expressions for  $v_c$  and  $K_c$  [given by Eqs. (B2) and (B3) with  $\lambda_1^* = \lambda_2 = 0$ ], one can rewrite the results in a form that shows more clearly how the relation  $v_c^*/v_c = K_c/K_c^* = \sqrt{1 - \lambda}$  is modified by the presence of el-ph backscattering—see Eqs. (24) and (25). There, the effects of el-ph backscattering are contained in the parameter  $\Lambda$ , defined in Eq. (26).

- 
- <sup>1</sup> A. Lanzara, P. V. Bogdanov, X. J. Zhou, S. A. Kellar, D. L. Feng, E. D. Lu, T. Yoshida, H. Eisaki, A. Fujimori, K. Kishio, J.-I. Shimoyama, T. Noda, S. Uchida, Z. Hussain, and Z.-X. Shen, *Nature (London)* **412**, 510 (2001).
- <sup>2</sup> X. J. Zhou, T. Yoshida, A. Lanzara, P. V. Bogdanov, S. A. Kellar, K. M. Shen, W. L. Yang, F. Ronning, T. Sasagawa, T. Kakeshita, T. Noda, H. Eisaki, S. Uchida, C. T. Lin, F. Zhou, J. W. Xiong, W. X. Ti, Z. X. Zhao, A. Fujimori, Z. Hussain, and Z.-X. Shen, *Nature (London)* **423**, 398 (2003).
- <sup>3</sup> G.-H. Gweon, T. Sasagawa, S. Y. Zhou, J. Graf, H. Takagi, D.-H. Lee, and A. Lanzara, *Nature (London)* **430**, 187 (2004).
- <sup>4</sup> P. W. Anderson, *The Theory of Superconductivity in the High- $T_c$  Cuprates* (Princeton University Press, Princeton, NJ, 1997).
- <sup>5</sup> D. Orgad, S. A. Kivelson, E. W. Carlson, V. J. Emery, X. J. Zhou, and Z.-X. Shen, *Phys. Rev. Lett.* **86**, 4362 (2001).
- <sup>6</sup> M. Vojta, Y. Zhang, and S. Sachdev, *Int. J. Mod. Phys. B* **14**, 3719 (2000).
- <sup>7</sup> T. Valla, A. V. Fedorov, P. D. Johnson, B. O. Wells, S. L. Hulbert, Q. Li, G. D. Gu, and N. Koshizuka, *Science* **285**, 2110 (1999).
- <sup>8</sup> V. Meden, K. Schönhammer, and O. Gunnarsson, *Phys. Rev. B* **50**, 11179 (1994).
- <sup>9</sup> C. Bourbonnais, in *High Magnetic Fields: Applications in Condensed Matter Physics and Spectroscopy*, edited by C. Berthier, L. P. Levy, and G. Martinez (Springer-Verlag, Berlin, 2002), p. 235.
- <sup>10</sup> R. Egger, A. Bachtold, M. Fuhrer, M. Bockrath, D. Cobden, and P. McEuen, in *Interacting Electrons in Nanostructures*, edited by R. Haug and H. Schoeller (Springer-Verlag, Berlin, 2001), p. 125.
- <sup>11</sup> G.-H. Gweon, J. D. Denlinger, J. W. Allen, R. Claessen, C. G. Olson, H. Höchst, J. Marcus, C. Schlenker, L. F. Schneemeyer, and G. Gweon, *J. Electron Spectrosc. Relat. Phenom.* **117**, 481 (2001).
- <sup>12</sup> J. W. Allen, *Solid State Commun.* **123**, 469 (2002).
- <sup>13</sup> G.-H. Gweon, J. W. Allen, and J. D. Denlinger, *Phys. Rev. B* **68**, 195117 (2003).
- <sup>14</sup> For a recent review of the experimental evidence regarding the existence of local stripe correlations in the high-temperature superconductors, see S. A. Kivelson, I. P. Bindloss, E. Fradkin, V. Oganesyan, J. M. Tranquada, A. Kapitulnik, and C. Howald, *Rev. Mod. Phys.* **75**, 1201 (2003).
- <sup>15</sup> In the present paper, we compare our results to ARPES measurements in the cuprates in the nodal direction  $\mathbf{k} = (0,0)-(\pi,\pi)$ . This is done without microscopic justification. However, it is worth mentioning that in Refs. 43 and 44, the band structure of a disordered array of stripes is computed, and is found to have a nodal component. This implies that the 1D physics along the stripes is being mirrored in this direction. We also mention that, according to Ref. 45, effective 1D physics can emerge in a 2D system with straight Fermi segments and strong interactions.
- <sup>16</sup> For a recent review, see F. Marsiglio and J. P. Carbotte, cond-mat/0106143 (unpublished).
- <sup>17</sup> We do not mean to imply that phonons produce no broadening at high binding energies in the LL. They indeed do, in a way analogous to the Fermi liquid, but for  $K_c \ll 1$  this effect is negligible compared to the huge amount of broadening already present in the EDCs from direct el-el interactions. In contrast, the narrowing effect for  $|E| < \omega_0$ , due to an increase in the effective  $K_c$ , is dramatic in the LL but not present in the Fermi liquid.
- <sup>18</sup> V. J. Emery, in *Highly Conducting One-Dimensional Solids*, edited by J. T. Devreese, R. P. Evrard, and V. E. van Doren (Plenum, New York, 1979), p. 247.
- <sup>19</sup> E. Fradkin, *Field Theories of Condensed Matter Systems* (Addison-Wesley, Reading, MA, 1991).
- <sup>20</sup> J. Voit, *Rep. Prog. Phys.* **58**, 977 (1995).
- <sup>21</sup> A. O. Gogolin, A. A. Nersesyan, and A. M. Tsvelik, *Bosonization and Strongly Correlated Systems* (Cambridge University Press, Cambridge, U.K., 1998).
- <sup>22</sup> T. Giamarchi, *Quantum Physics in One Dimension* (Oxford University Press, Oxford, 2004).
- <sup>23</sup> D. Loss and T. Martin, *Phys. Rev. B* **50**, 12160 (1994).
- <sup>24</sup> For the spectral function in the absence of electron-phonon coupling, see A. Luther and I. Peschel, *Phys. Rev. B* **9**, 2911 (1974); V. J. Emery, in *Highly Conducting One-Dimensional Solids* (Ref. 18); V. Meden and K. Schönhammer, *Phys. Rev. B* **46**, 15753 (1992); J. Voit, *Phys. Rev. B*, **47**, 6740 (1993); D. Orgad, *Philos. Mag. B* **81**, 375 (2001); T. Giamarchi, *Quantum Physics in One Dimension* (Ref. 22).
- <sup>25</sup> The single-hole spectral function for  $k$  near  $-k_F$  is given by  $A(-k, E)$ . The *single-particle* spectral function for  $k$  near  $\pm k_F$  is  $A(\mp k, -E)$ . The full spectral function for  $k$  near  $\pm k_F$  is given by  $A(\pm k, E) + A(\mp k, -E)$ .

- <sup>26</sup> We plot the spectral function in arbitrary units and therefore ignore the dependence of the numerical prefactor on  $\omega_0$ . The cutoff  $\bar{a}$  is also not considered a free parameter, since the spectral function is independent of its value so long as  $1/\bar{a} \gg |\bar{k}|, |\bar{E}|$ . For all plots, we used  $\bar{a} = 0.05$ .
- <sup>27</sup> A. Luther and V. J. Emery, Phys. Rev. Lett. **33**, 589 (1974).
- <sup>28</sup> I. P. Bindloss, cond-mat/0404154 (unpublished).
- <sup>29</sup> It is interesting to note that the instability at large  $\lambda$  mentioned in Sec. II survives the addition of el-ph backscattering, but is moved from  $\lambda = 1$  to  $\lambda = 1 + K_c^2 \Lambda$ .
- <sup>30</sup> P. V. Bogdanov, A. Lanzara, S. A. Kellar, X. J. Zhou, E. D. Lu, W. J. Zheng, G. Gu, J.-I. Shimoyama, K. Kishio, H. Ikeda, R. Yoshizaki, Z. Hussain, and Z. X. Shen, Phys. Rev. Lett. **85**, 2581 (2000).
- <sup>31</sup> A. Kaminski, M. Randeria, J. C. Campuzano, M. R. Norman, H. Fretwell, J. Mesot, T. Sato, T. Takahashi, and K. Kadowaki, Phys. Rev. Lett. **86**, 1070 (2001).
- <sup>32</sup> P. D. Johnson, T. Valla, A. V. Fedorov, Z. Yusof, B. O. Wells, Q. Li, A. R. Moodenbaugh, G. D. Gu, N. Koshizuka, C. Kendziora, Sha Jian, and D. G. Hinks, Phys. Rev. Lett. **87**, 177007 (2001).
- <sup>33</sup> Some authors have suggested that a part of the measured  $A(\mathbf{k}, E)$  is due to extrinsic processes which also produce a “background” signal at wave vectors far outside the Fermi surface. If such a background is subtracted from the measured signals, it reduces, but does not eliminate the long high energy tails seen in the EDCs. We believe that good fits could be obtained to the data in this case, too, although likely with somewhat smaller values of  $\gamma_c$ .
- <sup>34</sup> A. Kaminski, J. Mesot, H. Fretwell, J. C. Campuzano, M. R. Norman, M. Randeria, H. Ding, T. Sato, T. Takahashi, T. Mochiku, K. Kadowaki, and H. Hoehst, Phys. Rev. Lett. **84**, 1788 (2000).
- <sup>35</sup> For 2D or 3D systems that contain a kink due to el-ph coupling, the dispersion at high binding energies is seen to extrapolate to the origin in both theory (Ref. 37) and experiment (Ref. 46).
- <sup>36</sup> T. Yoshida, X. J. Zhou, T. Sasagawa, W. L. Yang, P. V. Bogdanov, A. Lanzara, Z. Hussain, T. Mizokawa, A. Fujimori, H. Eisaki, Z.-X. Shen, T. Kakeshita, and S. Uchida, Phys. Rev. Lett. **91**, 027001 (2003).
- <sup>37</sup> S. Verga, A. Knigavko, and F. Marsiglio, Phys. Rev. B **67**, 054503 (2003).
- <sup>38</sup> E. Schachinger, J. J. Tu, and J. P. Carbotte, Phys. Rev. B **67**, 214508 (2003).
- <sup>39</sup> T. Martin and D. Loss, Int. J. Mod. Phys. B **9**, 495 (1995).
- <sup>40</sup> The single-particle density of states (momentum integrated spectral function) for a different model of a LL coupled to acoustic phonons was investigated in Ref. 47.
- <sup>41</sup> G. T. Zimanyi, S. A. Kivelson, and A. Luther, Phys. Rev. Lett. **60**, 2089 (1988).
- <sup>42</sup> J. Voit and H. J. Schulz, Phys. Rev. B **37**, 10068 (1988).
- <sup>43</sup> M. Granath, V. Oganessian, D. Orgad, and S. A. Kivelson, Phys. Rev. B **65**, 184501 (2002).
- <sup>44</sup> M. Granath, Phys. Rev. B **69**, 214433 (2004).
- <sup>45</sup> A. Luther, Phys. Rev. B **50**, 11446 (1994).
- <sup>46</sup> T. Valla, A. V. Fedorov, P. D. Johnson, and S. L. Hulbert, Phys. Rev. Lett. **83**, 2085 (1999).
- <sup>47</sup> E. Papa and A. M. Tsvelik, cond-mat/0004007 (unpublished).